

# Audio-Visual World Models: Towards Multisensory Imagination in Sight and Sound

Jiahua Wang<sup>1\*</sup> Shannan Yan<sup>1\*</sup> Leqi Zheng<sup>1\*</sup> Jialong Wu<sup>1</sup> Yaoxin Mao<sup>2</sup>

<sup>1</sup>Tsinghua University

<sup>2</sup>Beijing Institute of Technology

## Abstract

World models simulate environmental dynamics to enable agents to plan and reason about future states. While existing approaches have primarily focused on visual observations, real-world perception inherently involves multiple sensory modalities. Audio provides crucial spatial and temporal cues such as sound source localization and acoustic scene properties, yet its integration into world models remains largely unexplored. No prior work has formally defined what constitutes an audio-visual world model or how to jointly capture binaural spatial audio and visual dynamics under precise action control with task reward prediction. This work presents the first formal framework for Audio-Visual World Models (AVWM), formulating multimodal environment simulation as a partially observable Markov decision process with synchronized audio-visual observations, fine-grained actions, and task rewards. To address the lack of suitable training data, we construct AVW-4k, a dataset comprising 30 hours of binaural audio-visual trajectories with action annotations and reward signals across 76 indoor environments. We propose AV-CDiT, an Audio-Visual Conditional Diffusion Transformer with a novel modality expert architecture that balances visual and auditory learning, optimized through a three-stage training strategy for effective multimodal integration. Extensive experiments demonstrate that AV-CDiT achieves high-fidelity multimodal prediction across visual and auditory modalities with reward. Furthermore, we validate its practical utility in continuous audio-visual navigation tasks, where AVWM significantly enhances the agent’s performance.

## 1. Introduction

In recent years, large-scale pre-trained models have significantly advanced a wide range of AI applications. A natural extension of this success is to equip models with the ability to predict and reason about future states of the world. In this context, world models [9, 14, 16, 39, 42] have emerged as

\*These authors contributed equally.

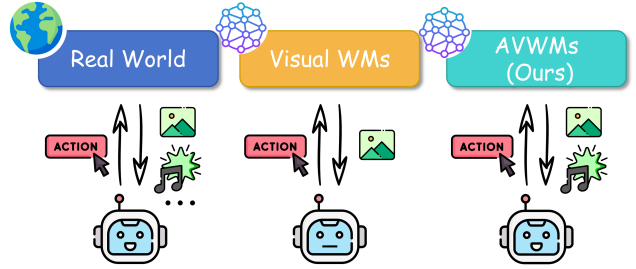


Figure 1. **From unimodal to audio-visual world models.** While embodied agents in the real world perceive through multiple sensory modalities including vision and audio, existing world models predominantly focus on visual observations alone. Our work introduces Audio-Visual World Models (AVWMs), the first framework to jointly simulate synchronized audio-visual dynamics under precise action control with task reward prediction.

a fundamental paradigm for enabling AI systems to understand and simulate environmental dynamics. World models aim to encode the underlying dynamics of an environment, allowing an agent to predict future observations and rewards based on its actions, thereby providing a foundation for planning, decision making, and reasoning in complex environments. While early world modeling efforts predominantly focused on visual observations, real-world perception is inherently multimodal. Among the various sensory modalities, audio carries rich information about environmental properties that are often complementary to visual cues [10, 29, 40, 41]. For instance, the spatial location of sound sources, the acoustic characteristics of physical spaces, and the temporal evolution of auditory events all provide critical signals for embodied agents navigating and interacting with their surroundings. As such, developing world models that can jointly capture audio-visual dynamics under precise action control represents an essential step toward building intelligent agents capable of human-like environmental understanding.

However, existing research faces two major limitations that hinder progress toward multimodal world modeling.

**Limitation 1: Conceptual and data-level gap in constructing audio-visual world models.** Although multi-

Table 1. Comparison with existing world modeling approaches. Our work is the first to achieve precise action control, binaural spatial audio modeling, and reward prediction in a unified framework.

Method	Modality	Precise Action	Binaural Audio	Reward
DIAMOND [2]	Visual	✓	✗	✓
Genie [6]	Visual	✗	✗	✗
Cosmos [1]	Visual	✗	✗	✗
VLWM [37]	Visual+Text	✗	✗	✗
RLVR-World [33]	Visual+Text	✓	✗	✓
WorldGPT [13]	Visual+Audio	✗	✗	✗
AV-CDiT (Ours)	Visual+Audio	✓	✓	✓

modal perception has become a central goal for embodied intelligence, there remains no formalized definition of what constitutes an audio-visual world model. Prior work has not clarified how synchronized audio and visual observations, fine-grained actions, and task rewards should be jointly modeled within a unified world-dynamics formulation. There is also a lack of standardized datasets. Existing datasets are either purely visual or provide entire audio and video tracks that lack action-conditioned correspondence. Besides they hardly capture spatial acoustic characteristics, making them unsuitable for constructing and evaluating controllable audio-visual world models.

**Limitation 2: Architectural gap in modeling controllable multimodal dynamics.** Even if such a formulation were available, current modeling paradigms remain inadequate for learning coherent and controllable multimodal world dynamics. As summarized in Table 1, existing world models either focus solely on visual dynamics or incorporate audio without fine-grained action conditioning, spatial acoustic reasoning, and reward prediction. Although some multimodal world model architectures extend beyond vision to incorporate modalities such as text, they are primarily designed to capture semantic associations rather than temporally aligned sensory dynamics. Consequently, these architectures remain inadequate for audio-visual world modeling, where the audio modality is inherently synchronized with visual signals over time.

As illustrated in Figure 1, while real-world embodied agents naturally perceive through both visual and auditory channels, existing world models remain confined to unimodal visual prediction. This raises a critical question: *How can we formally define and implement an audio-visual world model that accurately captures synchronized multimodal dynamics under precise action control while predicting environmental feedback?*

To bridge these gaps, we re-examine world modeling from a multimodal perspective, arguing that a genuine world model must capture how actions propagate through both the visual and acoustic domains over time. Our contributions are threefold:

- **Formal Problem Formulation and Dataset:** To address

the first limitation, we provide the first formal definition of Audio-Visual World Models (AVWM), establishing a unified framework for modeling binaural spatial audio, visual observations, precise action control, and task rewards within a POMDP formulation. To support this formulation, we construct AVW-4k, comprising approximately 30 hours of synchronized binaural audio-visual data with action annotations and reward signals across 76 indoor environments (Section 3).

- **Modality Expert with Stagewise Training:** To address the second limitation, we design AV-CDiT, an Audio-Visual Conditional Diffusion Transformer featuring a novel modality expert architecture that balances cross-modal interaction while preserving modality-specific representations. We further develop a three-stage training strategy that ensures stable optimization and enhances multimodal integration (Section 4).
- **Comprehensive Experimental Validation:** We conduct extensive experiments demonstrating that our model achieves high-fidelity multimodal prediction across visual, auditory, and reward modalities, and serves as an effective planning tool for continuous audio-visual navigation tasks, validating its utility for downstream embodied AI applications (Section 5).

## 2. Related Works

**Multimodal World Models.** The world models are expected to simulate real-world dynamics by accumulating commonsense knowledge about how the world [32]. Earlier unimodal world models [2, 15, 24] primarily focused on visual prediction. However, real-world perception is inherently multimodal, involving not only vision but also language [22, 33, 37] and audio [13]. Meanwhile, WorldGPT [13] incorporates audio into scene generation but remains reward-agnostic and lacks explicit modeling or control of fine-grained agent actions, relying mainly on weak semantic supervision; as a result, it functions more as an audiovisual conditional generator than a controllable multimodal world model. This gap underscores the need for a unified model that jointly captures visual and auditory dynamics under precise action control and predicts task-level rewards for interaction-aware, high-fidelity world simulation.

**Audiovisual Generation.** Audiovisual generation tasks encompass cross modal generation (e.g., audio to video), multimodal interpolation, and audiovisual continuation [20]. The latter two tasks generally provide a temporally aligned audiovisual segment as conditioning and require the model to predict or fill in a specified portion of audio and video, ensuring that the entire sequence remains temporally coherent. Recent works [20, 28, 34] have proposed more versatile audiovisual models to address these tasks. However, compared with world models, such generative models gen-

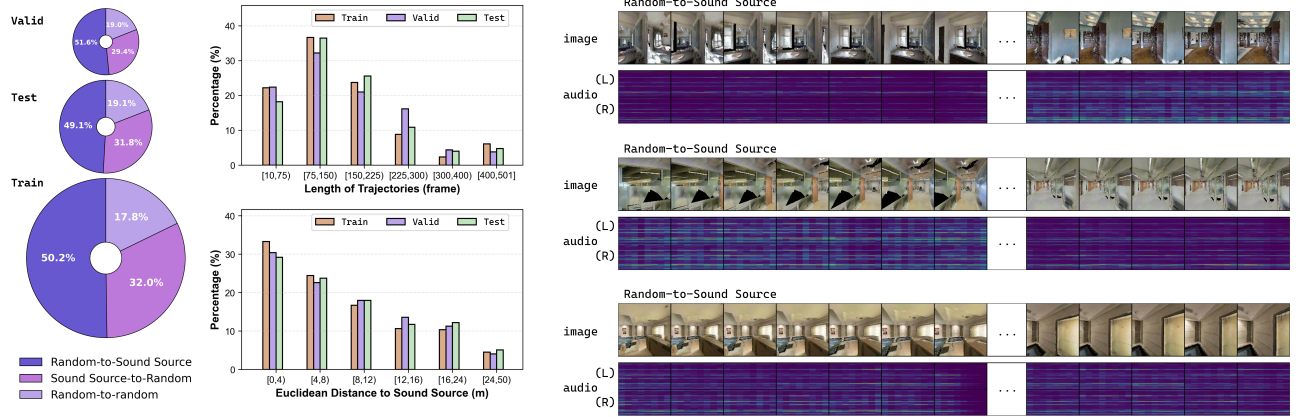


Figure 2. Dataset statistics and trajectory examples of the proposed AVW-4k. **Left:** Proportions of trajectories corresponding to the three motion patterns in the train/validation/test splits. **Middle:** Distributions of trajectory lengths and geodesic distances to the sound source across all frames in the dataset. **Right:** Representative trajectories for each motion pattern, with audios shown as binaural spectrograms.

erate specific content conditioned merely on given frames. While world models explicitly model action-conditioned state transitions and thus perform counterfactual reasoning. This enables them to answer questions of the form ‘What would have happened if the agent had taken a different action?’, rather than merely ‘What will happen next?’. Nonetheless, these generative models have undeniably provided valuable insights and inspiration for the development of the audiovisual world model proposed in this work.

### 3. Formulation and Dataset Construction

#### 3.1. Audio-Visual World Models

An Audio-Visual World Model (AVWM) is designed to simulate an external environment containing sound signals. In this environment there exists a stationary sound source. We model this environment as a partially observable Markov decision process (POMDP), defined as a tuple  $(\mathcal{S}, \mathcal{O}, \mathcal{A}, p, r)$ . At each time step  $t$ ,  $s_t \in \mathcal{S}$  represents the underlying state of the environment.  $o_t = \phi(s_t) = \{o_t^v, o_t^a\} \in \mathcal{O}$  represents the partial observation received by the agent, only providing incomplete information of  $s_t$ .  $o_t^v \in \mathbb{R}^{H \times W \times 3}$  is the visual observation (an image frame) and  $o_t^a \in \mathbb{R}^{L \times 2}$  is the binaural auditory observation (a short segment of binaural audio). Action  $a_t = (u_t, \omega_t) \in \mathcal{A}$  specifies a spatial transformation of the agent, where  $u_i$  and  $\omega_i$  denote the positional and orientational transformations, respectively.

Note that all actions in the discrete action space  $\mathcal{A}$  are executed with the same time duration. When  $a_t$  is executed at time step  $t$ , the environment transitions according to  $p(s_{t+1} | s_t, a_t)$ , producing new audio-visual observations and an immediate reward  $r_{t+1} = r(s_t, a_t)$ . In our formulation, the reward provides environmental feedback reflecting task progress, enabling the model to associate ac-

tions with both perceptual changes and task outcomes. For example, in navigation tasks, it can be defined by the reduction in shortest-path distance to the target.

In order to simulate the the aforementioned environment, we describe an AVWM as follows:

$$\hat{o}_{t+\Delta t}, \hat{r}_{t+\Delta t} \sim p_{\theta}(o_{t+\Delta t}, r_{t+\Delta t} | o_{t-m+1:t}, a_{t \rightarrow t+\Delta t}, \Delta t), \quad (1)$$

where  $o_{t-m+1:t}$  denotes the current observation along with its preceding frames, collectively referred to as the  $m$ -frame context.  $a_{t \rightarrow t+\Delta t}$  denotes the spatial vector sum of the action sequence  $a_{t:t+\Delta t}$  from the current frame  $o_t$  to the target frame  $o_{t+\Delta t}$ .  $\Delta t \in [T_{\min}, T_{\max}]$  specifies the temporal offset measured in frames, and  $\hat{r}_{t+\Delta t}$  denotes the cumulative reward predicted over this interval.

The idea of conducting skip-step prediction by varying the temporal offset  $\Delta t$  follows [4], allowing the model not only to perform next-frame prediction. Such temporal abstraction enables the world model to learn how the environment evolves over different time horizons, thereby improving its understanding of long-term spatio-temporal dependencies and underlying physical dynamics.

#### 3.2. AVW-4k Dataset

To train and evaluate our model, we construct AVW-4k, an audio-visual interaction dataset collected in simulated indoor environments.

**Data Collection.** Data collection is conducted within the simulation environment built upon the Matterport3D dataset [7] and the SoundSpaces 2.0 simulator [8]. This allows for physically accurate sound propagation with frequency-dependent acoustic effects such as reflection, absorption, and reverberation.

During data collection, an agent continuously moves within the simulated 3D scenes while recording synchronized auditory and visual observations at each timestep.

Each environment contains a stationary sound source fixed at a known location, which continuously plays a looping telephone ringtone. The agent’s trajectories are randomly sampled according to three motion patterns: (1) moving from the source to a random goal position, (2) moving from a random start position toward the source, and (3) moving between two random positions independent of the source. All trajectories are ensured to be navigable and maintain a reasonable distance from the source to prevent silent recordings.

Each frame consists of an egocentric RGB image with a resolution of  $128 \times 128$  pixels and a 0.15-second binaural audio segment sampled at 16 kHz, strictly time-aligned across modalities. The action space of AVW-4k include four actions: move forward by 0.15 m, turn left by  $10^\circ$ , turn right by  $10^\circ$  and stop. AVW-4k provides a task reward between two consecutive frames by using the reduction in the shortest-path distance to the sound source. Each sample contains no more than 500 frames.

**Dataset Composition.** The final AVW-4k dataset contains approximately 30 hours of audio-visual data, spanning 76 indoor scenes and 4,500 trajectories. Trajectory lengths vary depending on navigation paths and acoustic configurations. The dataset is divided into training, validation, and test splits with a ratio of 6 : 1 : 2, where the environments across subsets are non-overlapping, ensuring a fair evaluation of the model’s cross-scene generalization ability.

## 4. Methodology

To implement the aforementioned AVWM, we design an integrated framework with two key innovations: the Audio-Visual Conditional Diffusion Transformer (AV-CDiT) featuring a novel modality expert architecture (Section 4.1), and a stagewise training strategy (Section 4.2).

### 4.1. Audio-Visual Conditional Diffusion Transformer

**Model Architecture.** AV-CDiT is a temporally autoregressive Transformer model capable of generating both visual and auditory frames, while additionally supporting the prediction of task reward. Building upon prior advances such as CDiT [4], which was originally developed for unimodal visual world models, AV-CDiT extends the diffusion framework to support action-conditioned multimodal generation through a novel architecture, illustrated in Figure 3.

AV-CDiT first employs two pre-trained and frozen encoders to encode visual frames  $o^v$  and auditory segments  $o^a$ , obtaining their respective latent representations  $z^v$  and  $z^a$ , similar in spirit to latent diffusion models [27].

Subsequently, latent representations from both modalities are projected into a shared latent space through separate adaptor layers for alignment. The scalar task reward  $r_{t+\Delta t}$

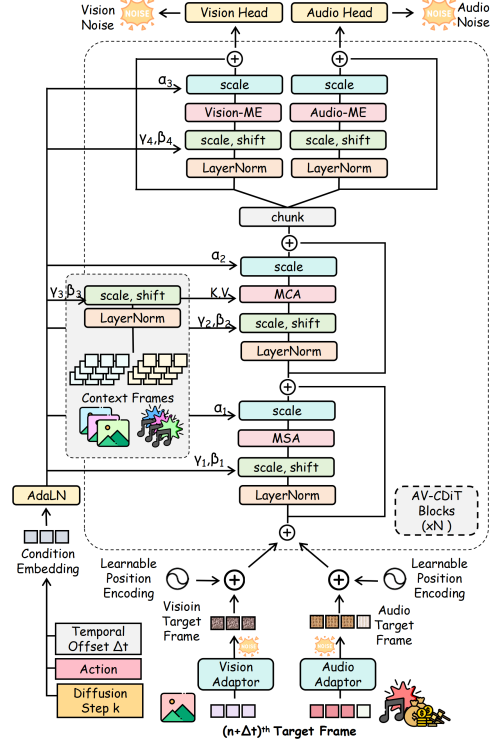


Figure 3. Overview of the proposed AV-CDiT architecture.

is then broadcast to match the token dimensionality as a reward token  $h_{t+\Delta t}^r$ . Finally, the visual, auditory, and reward tokens are concatenated to form the target sequence, which is noised during diffusion.

$$X_{t+\Delta t} = [h_{t+\Delta t}^v : h_{t+\Delta t}^a : h_{t+\Delta t}^r]. \quad (2)$$

This target sequence is subsequently fed into a stack of AV-CDiT blocks for multimodal diffusion-based generation.

Similar to the target sequence, the context sequence is constructed by concatenating context frames from both visual and auditory modalities.

$$C_{t-m+1:t} = [[h_{t-m+1}^v : h_{t-m+1}^a], \dots, [h_t^v : h_t^a]]. \quad (3)$$

The conditioning embedding is generated following the CDiT formulation. The aggregated action  $a_{t \rightarrow t+\Delta t}$ , temporal offset  $\Delta t$ , and diffusion timestep  $k$  are encoded via sinusoidal features and two-layer MLPs to obtain  $\psi_a$ ,  $\psi_{\Delta t}$ , and  $\psi_k$ , which are summed into a single conditioning vector  $c_t$ . This vector is then injected through an AdaLN [35] module to produce scale and shift parameters that modulate Layer Normalization and attention outputs, enabling conditional control during diffusion.

In each AV-CDiT Block, both visual and auditory tokens share common multi-head self-attention and cross-attention layers to enable joint modeling within a unified attention space. The self-attention layer facilitates cross-modal tem-



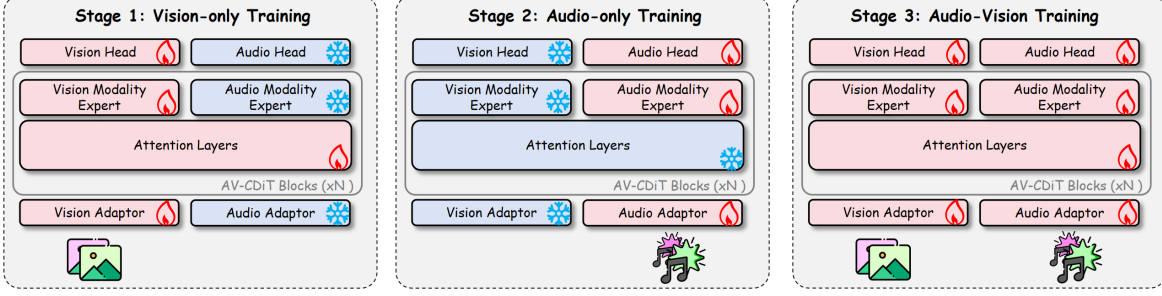


Figure 4. Illustration of the stagewise training strategy used for AV-CDiT.

poral coherence and semantic alignment, while the cross-attention layer conditions the fused target tokens on the context representations  $C_{t-m+1:t}$ , allowing each modality to exploit complementary information during generation.

**Modality Experts.** Inspired by previous expert network architectures [3, 31], each AV-CDiT block incorporates modality experts in the feed-forward layer that assign independent nonlinear mappings to each modality. After shared self-attention and cross-attention operations, the target sequence is divided into visual and auditory groups processed by corresponding modality expert sub-networks, with the reward token associated with the auditory branch, and outputs concatenated to reconstruct the unified sequence. This design prevents visual dominance from hindering auditory representation learning when leveraging visually pretrained models, enabling the auditory pathway to learn in a coordinated manner alongside the visual modality, which works in conjunction with the stage-wise training strategy in Section 4.2 and is validated in Section 5.3. After multiple stacked blocks, visual, auditory, and reward tokens are decoded through respective output heads to predict noise, with denoised tokens decoded into future observations and the reward token average-pooled to estimate future task reward.

**Diffusion Training.** We follow the DDPM [18] formulation to model future multimodal generation as a synchronized diffusion process across both visual and auditory-reward modalities. Given the clean latent targets  $X_{t+\Delta t}^v$  and  $X_{t+\Delta t}^{a:r}$ , Gaussian noise is independently injected into each modality according to a shared noise schedule  $\{\bar{\alpha}_k\}_{k=1}^K$ , while preserving their intrinsic correlation in the clean space:

$$\begin{aligned} X_{t+\Delta t}^{v,(k)} &= \sqrt{\bar{\alpha}_k} X_{t+\Delta t}^v + \sqrt{1 - \bar{\alpha}_k} \epsilon_v, \\ X_{t+\Delta t}^{a:r,(k)} &= \sqrt{\bar{\alpha}_k} X_{t+\Delta t}^{a:r} + \sqrt{1 - \bar{\alpha}_k} \epsilon_{a:r}, \end{aligned} \quad (4)$$

where  $\epsilon_v, \epsilon_{a:r} \sim \mathcal{N}(0, I)$  are modality-specific Gaussian noises.

This formulation assumes conditionally independent forward noising processes for the two modalities. Meanwhile, the multimodal dependency is retained in the reverse process through a unified denoising network.

The reverse process is parameterized by AV-CDiT, which

jointly predicts the injected noises  $(\hat{\epsilon}_v, \hat{\epsilon}_{a:r})$  in a single forward pass.

**Training Objective.** AV-CDiT adopts the standard  $\epsilon$ -prediction objective, estimating the noise added at each step rather than directly reconstructing clean targets. The loss is defined as:

$$\mathcal{L}_{\text{simple}} = \mathbb{E}_{k, \epsilon_v, \epsilon_{a:r}} [\|\hat{\epsilon}_v - \epsilon_v\|_2^2 + \|\hat{\epsilon}_{a:r} - \epsilon_{a:r}\|_2^2]. \quad (5)$$

Following [26], we predict the covariance matrix of the noise and supervise it with the variational lower-bound loss  $\mathcal{L}_{\text{vb}}$  [25], yielding the final objective  $\mathcal{L} = \mathcal{L}_{\text{simple}} + \lambda_{\text{vb}} \mathcal{L}_{\text{vb}}$ .

## 4.2. Stagewise Training Strategy

Inspired by previous work on multimodal joint pretrainings [3, 31], we adopt a three-stage training strategy to ensure stable optimization and efficient convergence of the multimodal diffusion model, illustrated in Figure 4.

In the first stage, the model is trained on vision-only data to learn spatial-temporal representations by jointly optimizing the self-attention layers, cross-attention layers, visual modality experts, visual adaptor layer, and visual head. In the second stage, only the auditory modality experts, auditory adaptor layer, and auditory head are fine-tuned on audio-only data while freezing all other components, including shared attention modules and vision-related layers, to preserve previously acquired visual capabilities and prevent strong visual priors from suppressing auditory representation learning. The reward token is incorporated into the auditory sequence to enable joint modeling of auditory patterns and their associated rewards. In the third stage, visual and auditory inputs are concatenated and the entire network undergoes end-to-end fine-tuning on synchronized audio-visual data, allowing all parameters to be jointly optimized for deeper multimodal fusion and improved consistency across generated visual frames, audio segments, and predicted rewards within the unified temporal diffusion process.

Table 2. Performance under **fixed-step** generation mode during training stages. We report the mean and standard deviation for each metric calculated over three runs. ' $\emptyset$ ' marks that the model does not produce outputs for this modality at this stage. Cell colors indicate relative performance compared to our final model (last row). Green and red shades denote better and worse results respectively, with color intensity reflecting the magnitude of the difference.

Training stages	Vision				Audio			Reward
	LPIPS $\downarrow$	DreamSim $\downarrow$	PSNR $\uparrow$	FID $\downarrow$	LSD $\downarrow$	SSIM $\uparrow$	FAD $\downarrow$	MSE $\downarrow$
Pretrained NWM	0.628 $\pm$ 0.000	0.516 $\pm$ 0.000	11.828 $\pm$ 0.001	89.412 $\pm$ 0.058	$\emptyset$	$\emptyset$	$\emptyset$	$\emptyset$
Training Stage 1	0.382 $\pm$ 0.000	0.258 $\pm$ 0.000	16.539 $\pm$ 0.001	25.906 $\pm$ 0.034	$\emptyset$	$\emptyset$	$\emptyset$	$\emptyset$
Training Stage 1+2	$\emptyset$	$\emptyset$	$\emptyset$	$\emptyset$	1.297 $\pm$ 0.000	0.531 $\pm$ 0.000	2.684 $\pm$ 0.001	0.889 $\pm$ 0.006
<b>Training Stage 1+2+3 (ours)</b>	0.382 $\pm$ 0.000	0.255 $\pm$ 0.000	16.504 $\pm$ 0.005	24.347 $\pm$ 0.023	1.311 $\pm$ 0.000	0.547 $\pm$ 0.000	2.391 $\pm$ 0.001	0.746 $\pm$ 0.002

Table 3. Performance under **rollout** generation mode during training stages. Other settings are the same as the Table 2.

Training stages	Vision				Audio			Reward
	LPIPS $\downarrow$	DreamSim $\downarrow$	PSNR $\uparrow$	FID $\downarrow$	LSD $\downarrow$	SSIM $\uparrow$	FAD $\downarrow$	MSE $\downarrow$
Pretrained NWM	0.667 $\pm$ 0.000	0.557 $\pm$ 0.000	11.435 $\pm$ 0.008	87.335 $\pm$ 0.097	$\emptyset$	$\emptyset$	$\emptyset$	$\emptyset$
Training Stage 1	0.414 $\pm$ 0.000	0.278 $\pm$ 0.000	15.941 $\pm$ 0.005	26.227 $\pm$ 0.032	$\emptyset$	$\emptyset$	$\emptyset$	$\emptyset$
Training Stage 1+2	$\emptyset$	$\emptyset$	$\emptyset$	$\emptyset$	1.628 $\pm$ 0.000	0.544 $\pm$ 0.000	1.645 $\pm$ 0.004	0.062 $\pm$ 0.000
<b>Training Stage 1+2+3 (ours)</b>	0.407 $\pm$ 0.000	0.272 $\pm$ 0.000	16.019 $\pm$ 0.006	23.871 $\pm$ 0.073	1.620 $\pm$ 0.000	0.577 $\pm$ 0.000	1.315 $\pm$ 0.002	0.052 $\pm$ 0.000

## 5. Experiments and Results

### 5.1. Experimental Setting

**Evaluation Metrics.** For the image results, following prior works on unimodal visual world models [4, 33], we apply LPIPS [38] and DreamSim [12] to measure perceptual similarity between predicted and ground-truth frames based on deep visual features, PSNR for pixel-level quality, and Fréchet Inception Distance (FID) [17] to evaluate the generated data distribution.

For the audio results, since the AVWM formulation requires a much higher degree of temporal and perceptual consistency between the generated and ground-truth audio than typical audiovisual generation tasks [20, 28], we adopt not only Fréchet Audio Distance (FAD) [19] to assess overall audio realism, but also several fine-grained metrics commonly used in audio-related generation tasks such as speech restoration [23], and audio super-resolution [21]. Specifically, we compute Log-Spectral Distance (LSD) [11] to evaluate frequency-domain deviation and Spectral Structural Similarity (SSIM) [30] to measure structural coherence between predicted and reference spectrograms. Since our model generates binaural audio, all audio metrics are computed independently on each channel and then averaged. Additionally, for FAD evaluation, both the generated and ground-truth audio signals are zero-padded to ensure compatibility with the VGGish model used for feature extraction.

For the reward prediction results, we directly employ the Mean Squared Error (MSE) as the evaluation metric.

**Encoder Configuration.** For the visual encoder, we use the Stable Diffusion [5] VAE tokenizer, similar to that employed in DiT [26] and CDiT. For the auditory encoder, we trained a SoundStream [36] tokenizer on AVW-4k, similar to that employed in AVDiT [20]. Notably, we remove one extraction block from the original SoundStream

encoder-decoder architecture to better accommodate the shorter audio segments in our dataset.

**Training Details.** For the implementation of the stage-wise training strategy, we first fine-tune a pretrained NWM model [4] of base size on the visual subset of the AVW-4k dataset. The model has been pre-trained on large-scale visual datasets and thus possesses certain visual reasoning capabilities. The parameters of its CDiT blocks, including those of the self-attention, cross-attention, and feed-forward layers, are then used to initialize the corresponding layers of an AV-CDiT model of identical size, marking the completion of the first stage of the stagewise training. Subsequently, we continue fine-tuning the model through the remaining two stages to complete the full stagewise training process.

The AV-CDiT model is trained with a context length of 4 frames. During training, each sample randomly selects 4 different navigation goals within a temporal window of  $\pm 16$  frames around the current timestep for prediction, following the training paradigm of CDiT.

We use the AdamW optimizer for training. The learning rates are set to  $1.6 \times 10^{-4}$ ,  $8 \times 10^{-4}$ , and  $1.6 \times 10^{-4}$  for the three stages of training. The total batch sizes for the three stages are 512, 768, and 128, respectively. All experiments are conducted on a single machine equipped with eight NVIDIA A100 GPUs.

### 5.2. Performance Evolution during Training Stages

**Setup.** We report the generative performance across the complete training stages, including a pre-trained NWM without training on AVW-4k, AV-CDiT fine-tuned on images (after stage 1), on audio with task reward (after stage 2), and jointly on both modalities (after stage 3).

For each experimental configuration, we perform prediction and evaluation under two generation modes. In the **fixed-step** generation mode, given a specified temporal off-

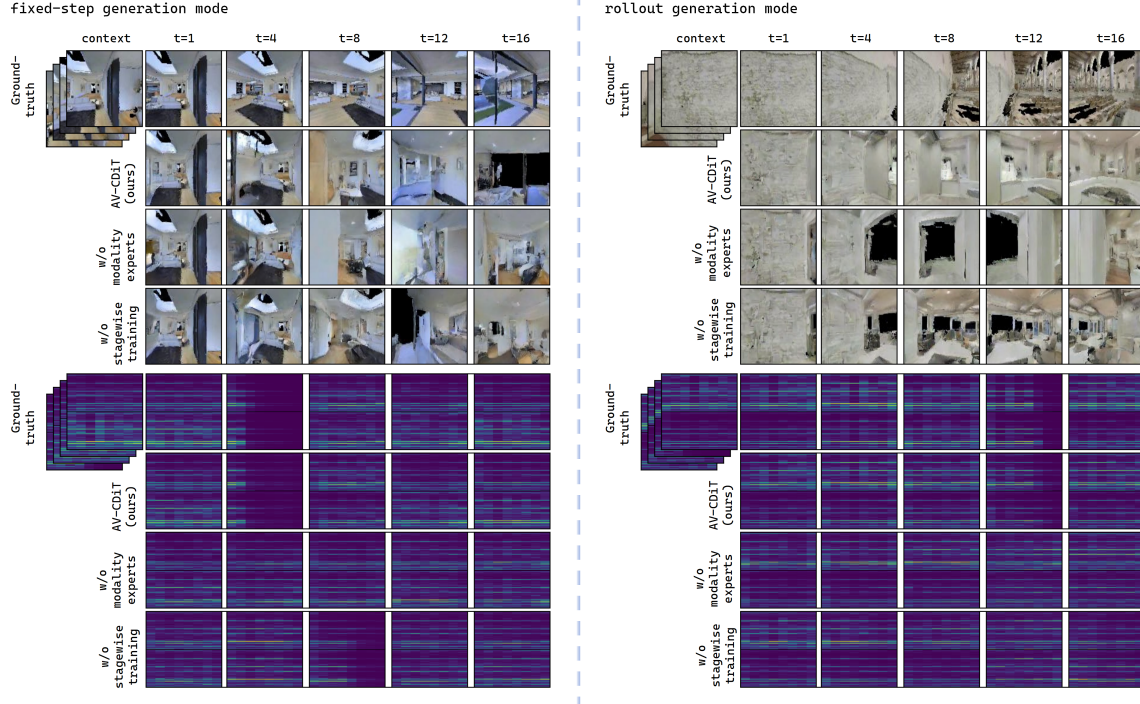


Figure 5. Qualitative analysis. **Left** and **right** respectively show image and audio generation results of our model and two ablated variants under the fixed-step and rollout modes.

Table 4. Ablation under **fixed-step** generation mode. We report the mean and standard deviation for each metric calculated over three runs. Cell colors indicate relative performance compared to our final model (last row). Green and red shades denote better and worse results respectively, with color intensity reflecting the magnitude of the difference.

Ablation	Vision				Audio			Reward
	LPIPS↓	DreamSim↓	PSNR↑	FID↓	LSD↓	SSIM↑	FAD↓	MSE↓
w/o modality experts	0.378 ± 0.000	0.253 ± 0.000	16.536 ± 0.002	24.342 ± 0.011	1.366 ± 0.000	0.485 ± 0.000	2.772 ± 0.001	1.357 ± 0.008
w/o stagewise training	0.380 ± 0.000	0.253 ± 0.000	16.545 ± 0.002	24.466 ± 0.007	1.371 ± 0.000	0.485 ± 0.000	2.758 ± 0.001	1.294 ± 0.006
<b>AV-CDiT (ours)</b>	0.382 ± 0.000	0.255 ± 0.000	16.504 ± 0.005	24.347 ± 0.023	1.311 ± 0.000	0.547 ± 0.000	2.391 ± 0.001	0.746 ± 0.002

Table 5. Ablation under **rollout** generation mode. Other settings are the same as the Table 4.

Ablation	Vision				Audio			Reward
	LPIPS↓	DreamSim↓	PSNR↑	FID↓	LSD↓	SSIM↑	FAD↓	MSE↓
w/o modality experts	0.403 ± 0.000	0.270 ± 0.000	16.013 ± 0.001	23.860 ± 0.072	1.668 ± 0.000	0.515 ± 0.000	2.007 ± 0.003	0.038 ± 0.000
w/o stagewise training	0.404 ± 0.000	0.269 ± 0.000	16.089 ± 0.004	24.180 ± 0.051	1.614 ± 0.000	0.507 ± 0.000	2.007 ± 0.007	0.040 ± 0.000
<b>AV-CDiT (ours)</b>	0.407 ± 0.000	0.272 ± 0.000	16.019 ± 0.006	23.871 ± 0.073	1.620 ± 0.000	0.577 ± 0.000	1.315 ± 0.002	0.052 ± 0.000

set  $\Delta t$ , the model directly predicts the outcome at frame  $t + \Delta t$ . We iterate  $\Delta t$  over a 16-frame horizon ahead of the current frame. In the **rollout** generation mode, the model performs autoregressive prediction, where each generated frame is recursively used as input to produce the subsequent frame until reaching frame  $t + 16$ .

**Results.** As shown in Tables 2 and 3, the three-stage training strategy effectively enables the model to maintain strong generative performance across both visual and auditory modalities.

After the first stage, the model’s visual generation quality improves substantially. After the second stage, the model develops the ability to reasoning on auditory modality and

generate plausible auditory outputs. After the third stage, the model not only retains the modality-specific knowledge learned in the previous stages-thus avoiding catastrophic forgetting-but also achieves better cross-modal alignment and joint representation learning, leading to further improvements in generation quality, particularly in the auditory modality.

### 5.3. Ablations

**Setup.** We conduct ablation studies to verify the effects of the modality experts and the stagewise training strategy. Specifically, we report the generative performance under two ablated settings. In the first setting, the modality ex-

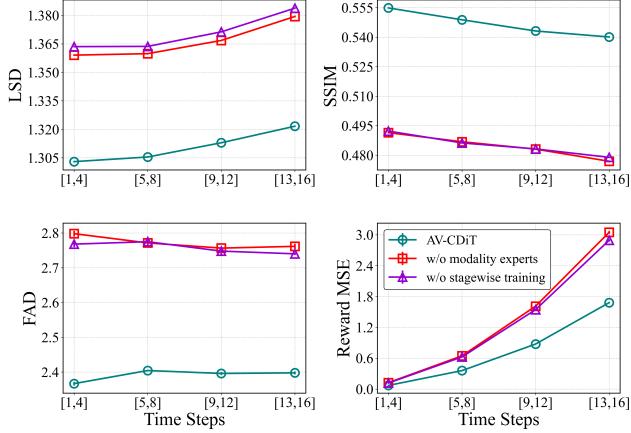


Figure 6. Temporal evolution of audio generation quality and reward prediction in step-fixed mode. The curves show the averaged performance of AV-CDiT and ablated variants over four future time-step intervals.

perts are removed and replaced with a shared feed-forward network, where the audio and visual token sequences are jointly processed. In the second setting, the modality experts are retained, but the model is directly fine-tuned on both modalities simultaneously. As in Section 5.2, we report results under both generation modes.

**Results.** As shown in Tables 4 and 5, after introducing modality experts and applying the stagewise training strategy, AV-CDiT maintains comparable generative performance in the visual modality, while exhibiting a remarkable improvement in the auditory modality. This result further validates our hypothesis that *both modality experts and stagewise training helps preserve the model’s visual generation capability while preventing the dominant visual representations from overwhelming the auditory branch*. In other words, this strategy effectively mitigates modality imbalance and enables the model to better learn and generate audio signals in a coordinated manner.

Figure 5 presents qualitative comparisons among AV-CDiT and its ablated variants under both generation modes, while Figure 6 illustrates the temporal evolution of audio and reward prediction metrics across time steps under step-fixed generation mode, highlighting consistent improvements of AV-CDiT over the ablated models.

#### 5.4. Planning with an Audio-Visual World Model

**Setup.** We evaluate the planning capability of AV-CDiT on the continuous audio-visual navigation (continuous AV-Nav) [8] task, where an agent navigates in a continuous 3D environment with egocentric RGB observations and binaural audio streams, and an episode is deemed successful if the agent issues a *stop* action within 1m of the target sound source.

Table 6. Performance improvement of the continuous AV-Nav agent with the integration of AVWM. ‘Oracle WM’ denotes an upper bound obtained by replacing the imagined audio-visual outcomes and predicted task reward from AVWM with the ground-truth environment feedback. Except for NA, all metrics have been converted to percentages.

AV-Nav Agent			SR $\uparrow$	SPL $\uparrow$	SoftSPL $\uparrow$	NA $\downarrow$	SNA $\uparrow$
$B = 3$	$k = 4$	AVWM	55.20	45.70	56.54	332.817	6.67
		Oracle WM	59.40	51.02	60.71	300.35	8.36
	$k = 5$	AVWM	<b>56.50</b>	<b>47.38</b>	56.53	<b>317.19</b>	<b>7.09</b>
		Oracle WM	60.10	51.98	61.44	297.68	8.53
$B = 4$	$k = 4$	AVWM	55.90	46.46	57.00	317.99	6.87
		Oracle WM	59.80	51.64	60.58	298.25	8.48
	$k = 5$	AVWM	56.40	46.74	<b>57.24</b>	<b>317.82</b>	<b>6.84</b>
		Oracle WM	58.70	50.50	60.58	301.52	8.17

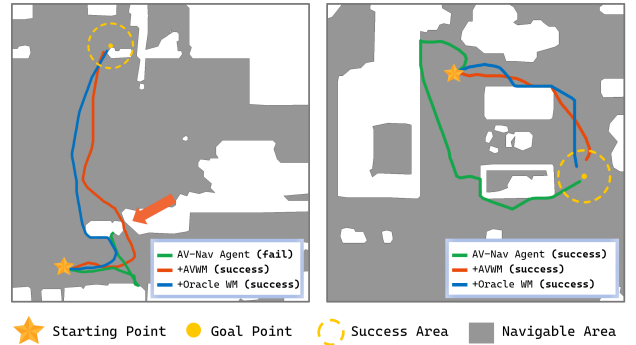


Figure 7. Comparison of navigation trajectories produced by three agents: the baseline AV-Nav agent (green), the AV-Nav agent enhanced with AVWM planning (red;  $n = 2$ ,  $B = 3$ ,  $k = 5$ ), and the upper-bound AV-Nav agent augmented with an oracle world model (blue).

The dataset of continuous AV-Nav is constructed on the SoundSpaces 2.0 simulation platform and the Matterport3D scenes, sharing the same action space as AVW-4k. The per-step reward consists of a success bonus, a constant negative step penalty, and the reduction in the shortest-path distance to the sound source, which aligns with the reward formulation used in AVW-4k. Therefore, the AVWM pretrained on AVW-4k can be directly applied to the continuous AV-Nav task without additional fine-tuning.

Specifically, we employ the following algorithm to enhance a pretrained baseline AV-Nav agent [8] using a trained AVWM.

At each environment timestep  $t$ , instead of sampling only one action from the current policy, the agent samples  $n$  candidate actions from its policy distribution. Each candidate action is then propagated through the world model for a  $k$ -step audio-visual rollout, producing predicted observations and rewards for the future sequence. At each rollout step, the predicted immediate reward from AVWM is combined with the policy network’s value estimation, discounted over



time, to compute the cumulative branch score. A beam search procedure is performed across rollout steps to retain up to  $B$  top-scoring action sequences. After the lookahead process is completed for the current timestep, the sequence with the highest cumulative score is selected, and its first action is executed in the real environment.

We report navigation performance under different beam widths  $B$  and rollout lengths  $k$  with the number of candidate actions to  $n = 2$ . The performance is evaluated using these common navigation metrics: success rate (SR), success weighted by path length (SPL), softSPL, number of actions (NA), and success normalized by action (SNA).

**Results.** As shown in Table 6, incorporating AVWM into the planning process effectively enhances the agent’s navigation performance under proper parameter configurations. In particular, the improvement in navigation efficiency, reflected by a significant reduction in the number of actions (NA), is especially pronounced. This is because AVWM enables the agent to evaluate multiple possible future outcomes before acting, leading to more informed and goal-directed decisions that reduce unnecessary exploration and shorten trajectories. Figure 7 illustrates a comparison of navigation trajectories under different settings.

## 6. Conclusion

In this paper, we introduced Audio-Visual World Models (AVWMs), a framework for simulating synchronized audio-visual dynamics under precise action control with task rewards. We constructed AVW-4k, a dataset of binaural audio-visual trajectories with fine-grained actions and rewards, and proposed AV-CDiT, a diffusion-based transformer with modality experts and stagewise training for balanced multimodal prediction. Our paradigm enables coherent and controllable simulation of multimodal futures and task-level reasoning. Moreover, by turning audio-visual imagination into forward action evaluation, AVWM provides a general mechanism for multisensory planning in embodied agents, advancing intelligent interaction in complex environments.

## References

- [1] Niket Agarwal, Arslan Ali, Maciej Bala, Yogesh Balaji, Erik Barker, Tiffany Cai, Prithvijit Chattopadhyay, Yongxin Chen, Yin Cui, Yifan Ding, et al. Cosmos world foundation model platform for physical ai. *arXiv preprint arXiv:2501.03575*, 2025. 2
- [2] Eloi Alonso, Adam Jelley, Vincent Micheli, Anssi Kanervisto, Amos Storkey, Tim Pearce, and François Fleuret. Diffusion for world modeling: Visual details matter in atari. In *Thirty-eighth Conference on Neural Information Processing Systems (NeurIPS)*, 2024. 2
- [3] Hangbo Bao, Wenhui Wang, Li Dong, Qiang Liu, Owais Khan Mohammed, Kriti Aggarwal, Subhojit Som, Songhao Piao, and Furu Wei. Vlmoe: Unified vision-language pre-training with mixture-of-modality-experts. *Advances in neural information processing systems*, 35:32897–32912, 2022. 5
- [4] Amir Bar, Gaoyue Zhou, Danny Tran, Trevor Darrell, and Yann LeCun. Navigation world models. In *Proceedings of the Computer Vision and Pattern Recognition Conference*, pages 15791–15801, 2025. 3, 4, 6
- [5] Andreas Blattmann, Tim Dockhorn, Sumith Kulal, Daniel Mendelevitch, Maciej Kilian, Dominik Lorenz, Yam Levi, Zion English, Vikram Voleti, Adam Letts, et al. Stable video diffusion: Scaling latent video diffusion models to large datasets. *arXiv preprint arXiv:2311.15127*, 2023. 6
- [6] Jake Bruce, Michael D Dennis, Ashley Edwards, Jack Parker-Holder, Yuge Shi, Edward Hughes, Matthew Lai, Aditi Mavalankar, Richie Steigerwald, Chris Apps, Yusuf Aytar, Sarah Bechtle, Feryal Behbahani, Stephanie Chan, Nicolas Heess, Lucy Gonzalez, Simon Osindero, Sherjil Ozair, Scott Reed, Jingwei Zhang, Konrad Zolna, Jeff Clune, Nando de Freitas, Satinder Singh, and Tim Rocktäschel. Genie: Generative interactive environments. In *Forty-first International Conference on Machine Learning (ICML)*, 2024. 2
- [7] Angel Chang, Angela Dai, Thomas Funkhouser, Maciej Halber, Matthias Niessner, Manolis Savva, Shuran Song, Andy Zeng, and Yinda Zhang. Matterport3d: Learning from rgb-d data in indoor environments. *arXiv preprint arXiv:1709.06158*, 2017. 3
- [8] Changan Chen, Carl Schissler, Sanchit Garg, Philip Kobernik, Alexander Clegg, Paul Calamia, Dhruv Batra, Philip Robinson, and Kristen Grauman. Soundspaces 2.0: A simulation platform for visual-acoustic learning. *Advances in Neural Information Processing Systems*, 35:8896–8911, 2022. 3, 8
- [9] Jintao Ding, Yunke Zhang, Yu Shang, Yuheng Zhang, Zefang Zong, Jie Feng, Yuan Yuan, Hongyuan Su, Nian Li, Nicholas Sukiennik, et al. Understanding world or predicting future? a comprehensive survey of world models. *ACM Computing Surveys*, 58(3):1–38, 2025. 1
- [10] Henghui Du, Guangyao Li, Chang Zhou, Chunjie Zhang, Alan Zhao, and Di Hu. Crab: A unified audio-visual scene understanding model with explicit cooperation. In *Proceedings of the Computer Vision and Pattern Recognition Conference*, pages 18804–18814, 2025. 1
- [11] Adoram Erell and Mitch Weintraub. Estimation using log-spectral-distance criterion for noise-robust speech recognition. In *International Conference on Acoustics, Speech, and Signal Processing*, pages 853–856. IEEE, 1990. 6
- [12] Stephanie Fu, Netanel Tamir, Shobhita Sundaram, Lucy Chai, Richard Zhang, Tali Dekel, and Phillip Isola. Dreamsim: Learning new dimensions of human visual similarity using synthetic data. *arXiv preprint arXiv:2306.09344*, 2023. 6
- [13] Zhiqi Ge, Hongzhe Huang, Mingze Zhou, Juncheng Li, Guoming Wang, Siliang Tang, and Yueting Zhuang. Worldgpt: Empowering llm as multimodal world model. In *Proceedings of the 32nd ACM International Conference on Multimedia*, pages 7346–7355, 2024. 2

- [14] Junliang Guo, Yang Ye, Tianyu He, Haoyu Wu, Yushu Jiang, Tim Pearce, and Jiang Bian. Mineworld: a real-time and open-source interactive world model on minecraft. *arXiv preprint arXiv:2504.08388*, 2025. 1
- [15] Danijar Hafner, Jurgis Pasukonis, Jimmy Ba, and Timothy Lillicrap. Mastering diverse domains through world models. *arXiv preprint arXiv:2301.04104*, 2023. 2
- [16] Danijar Hafner, Jurgis Pasukonis, Jimmy Ba, and Timothy Lillicrap. Mastering diverse control tasks through world models. *Nature*, pages 1–7, 2025. 1
- [17] Martin Heusel, Hubert Ramsauer, Thomas Unterthiner, Bernhard Nessler, and Sepp Hochreiter. Gans trained by a two time-scale update rule converge to a local nash equilibrium. *Advances in neural information processing systems*, 30, 2017. 6
- [18] Jonathan Ho, Ajay Jain, and Pieter Abbeel. Denoising diffusion probabilistic models. *Advances in neural information processing systems*, 33:6840–6851, 2020. 5
- [19] Kevin Kilgour, Mauricio Zuluaga, Dominik Roblek, and Matthew Sharifi. Fr\`echet audio distance: A metric for evaluating music enhancement algorithms. *arXiv preprint arXiv:1812.08466*, 2018. 6
- [20] Gwanghyun Kim, Alonso Martinez, Yu-Chuan Su, Brendan Jou, José Lezama, Agrim Gupta, Lijun Yu, Lu Jiang, Aren Jansen, Jacob Walker, et al. A versatile diffusion transformer with mixture of noise levels for audiovisual generation. *Advances in Neural Information Processing Systems*, 37:11837–11865, 2024. 2, 6
- [21] Chang Li, Zehua Chen, Liyuan Wang, and Jun Zhu. Audio super-resolution with latent bridge models. *arXiv preprint arXiv:2509.17609*, 2025. 6
- [22] Jessy Lin, Yuqing Du, Olivia Watkins, Danijar Hafner, Pieter Abbeel, Dan Klein, and Anca Dragan. Learning to model the world with language. *arXiv preprint arXiv:2308.01399*, 2023. 2
- [23] Haohe Liu, Qiuqiang Kong, Qiao Tian, Yan Zhao, DeLiang Wang, Chuanzeng Huang, and Yuxuan Wang. Voicefixer: Toward general speech restoration with neural vocoder. *arXiv preprint arXiv:2109.13731*, 2021. 6
- [24] Jingcheng Ni, Yuxin Guo, Yichen Liu, Rui Chen, Lewei Lu, and Zehuan Wu. Maskgwm: A generalizable driving world model with video mask reconstruction. In *Proceedings of the Computer Vision and Pattern Recognition Conference*, pages 22381–22391, 2025. 2
- [25] Alexander Quinn Nichol and Prafulla Dhariwal. Improved denoising diffusion probabilistic models. In *International conference on machine learning*, pages 8162–8171. PMLR, 2021. 5
- [26] William Peebles and Saining Xie. Scalable diffusion models with transformers. In *Proceedings of the IEEE/CVF international conference on computer vision*, pages 4195–4205, 2023. 5, 6
- [27] Robin Rombach, Andreas Blattmann, Dominik Lorenz, Patrick Esser, and Björn Ommer. High-resolution image synthesis with latent diffusion models. In *Proceedings of the IEEE/CVF conference on computer vision and pattern recognition*, pages 10684–10695, 2022. 4
- [28] Ludan Ruan, Yiyang Ma, Huan Yang, Huiguo He, Bei Liu, Jianlong Fu, Nicholas Jing Yuan, Qin Jin, and Baining Guo. Mm-diffusion: Learning multi-modal diffusion models for joint audio and video generation. In *Proceedings of the IEEE/CVF Conference on Computer Vision and Pattern Recognition*, pages 10219–10228, 2023. 2, 6
- [29] Hyeonngon Ryu, Seongyu Kim, Joon Son Chung, and Arda Senocak. Seeing speech and sound: Distinguishing and locating audios in visual scenes. *arXiv preprint arXiv:2503.18880*, 2025. 1
- [30] Zhou Wang, Alan C Bovik, Hamid R Sheikh, and Eero P Simoncelli. Image quality assessment: from error visibility to structural similarity. *IEEE transactions on image processing*, 13(4):600–612, 2004. 6
- [31] Chengyue Wu, Xiaokang Chen, Zhiyu Wu, Yiyang Ma, Xingchao Liu, Zizheng Pan, Wen Liu, Zhenda Xie, Xingkai Yu, Chong Ruan, et al. Janus: Decoupling visual encoding for unified multimodal understanding and generation. In *Proceedings of the Computer Vision and Pattern Recognition Conference*, pages 12966–12977, 2025. 5
- [32] Jialong Wu, Shaofeng Yin, Ningya Feng, Xu He, Dong Li, Jianye Hao, and Mingsheng Long. ivideopt: Interactive videogpts are scalable world models. *Advances in Neural Information Processing Systems*, 37:68082–68119, 2024. 2
- [33] Jialong Wu, Shaofeng Yin, Ningya Feng, and Mingsheng Long. Rlvr-world: Training world models with reinforcement learning. *arXiv preprint arXiv:2505.13934*, 2025. 2, 6
- [34] Yazhou Xing, Yingqing He, Zeyue Tian, Xintao Wang, and Qifeng Chen. Seeing and hearing: Open-domain visual-audio generation with diffusion latent aligners. In *Proceedings of the IEEE/CVF Conference on Computer Vision and Pattern Recognition*, pages 7151–7161, 2024. 2
- [35] Jingjing Xu, Xu Sun, Zhiyuan Zhang, Guangxiang Zhao, and Junyang Lin. Understanding and improving layer normalization. *Advances in neural information processing systems*, 32, 2019. 4
- [36] Neil Zeghidour, Alejandro Luebs, Ahmed Omran, Jan Skoglund, and Marco Tagliasacchi. Soundstream: An end-to-end neural audio codec. *IEEE/ACM Transactions on Audio, Speech, and Language Processing*, 30:495–507, 2021. 6
- [37] Peng-Fei Zhang, Ying Cheng, Xiaofan Sun, Shijie Wang, Lei Zhu, and Heng Tao Shen. A step toward world models: A survey on robotic manipulation. *arXiv preprint arXiv:2511.02097*, 2025. 2
- [38] Richard Zhang, Phillip Isola, Alexei A Efros, Eli Shechtman, and Oliver Wang. The unreasonable effectiveness of deep features as a perceptual metric. In *Proceedings of the IEEE conference on computer vision and pattern recognition*, pages 586–595, 2018. 6
- [39] Guosheng Zhao, Xiaofeng Wang, Zheng Zhu, Xinze Chen, Guan Huang, Xiaoyi Bao, and Xingang Wang. Drivedreamer-2: Llm-enhanced world models for diverse driving video generation. In *Proceedings of the AAAI Conference on Artificial Intelligence*, pages 10412–10420, 2025. 1

- [40] Xujian Zhao, Yixin Wang, and Peiquan Jin. Audio-visual adaptive fusion network for question answering based on contrastive learning. In *Proceedings of the AAAI Conference on Artificial Intelligence*, pages 10483–10491, 2025. [1](#)
- [41] Zhenghao Zhao, Hao Tang, and Yan Yan. Audio-visual navigation with anti-backtracking. In *International Conference on Pattern Recognition*, pages 358–372. Springer, 2025. [1](#)
- [42] Sicheng Zuo, Wenzhao Zheng, Yuanhui Huang, Jie Zhou, and Jiwen Lu. Gaussianworld: Gaussian world model for streaming 3d occupancy prediction. In *Proceedings of the Computer Vision and Pattern Recognition Conference*, pages 6772–6781, 2025. [1](#)